Wiley Online Library
Early View publication on www.wileyonlinelibrary.com
(issue and page numbers not yet assigned;
citable using Digital Object Identifier – **DOI**)

Phys. Status Solidi B, 1600779 (2017) / **DOI** 10.1002/pssb.201600779

physica status solidi b
www.pss-b.com
basic solid state physics

Formation, dissociation, and diffusion of various hydrogen dimers in silicon

Vladimir V. Voronkov* **and Robert Falster****

SunEdison Semiconductor, via Nazionale 59, 39012 Merano, Italy

Received 15 November 2016, revised 29 December 2016, accepted 13 January 2017
Published online 16 February 2017

Keywords boron, hydrogen, light-induced degradation, silicon

* Corresponding author: e-mail vvoronkov@sunedisonsemi.it, Phone: +39 0473 333 308, Fax: +39 0473 333 270
** e-mail rfalster@sunedisonsemi.it, Phone: +44 20 7704 9845, Fax: +44 1993 810806

Available data on hydrogen in silicon samples quenched from a high T and in those exposed to a plasma at low T are analyzed and the existence of three different forms of diatomic hydrogen is concluded. One of them, H_{2A} (a dimer of a moderate diffusivity) was fully characterized by the temperature dependence of its dissociation rate constant and its equilibrium constant and diffusivity. The two other forms, H_{2B} (of a high diffusivity) and H_{2C} (of a low diffusivity) are partially characterized. As a practical application of the properties of the dimers deduced here, the hydrogen content in solar cells was estimated from data on the permanent deactivation of boron–oxygen centers that degrade solar cell efficiency.

1 Introduction Hydrogen in silicon is a fascinating impurity. One reason for this is its ability to passivate dopants and other defects [1–4]. Another presumed hydrogen effect is to enhance [5–7] the permanent deactivation of boron–oxygen centers responsible for light-induced degradation (LID) of carrier lifetime [8–10]—an effect of primary importance for solar cell efficiency. The active hydrogen species in all these phenomena is definitely atomic hydrogen H which in boron-doped samples is mostly trapped by boron into HB neutral defects equilibrated with H [1–4]. However, in many cases the major part of the hydrogen is represented not by the active component HB + H but by a diatomic (dimeric) species H_2–leaving only a small hydrogen fraction to exist in its active form. Many, many papers have been devoted to hydrogen dimers in Si and yet the current state of understanding is not satisfactory. The situation is complicated by the existence of several structural forms of H_2 [3, 11–13]. In the present paper, we analyze available experimental data on H_2 and conclude that there are at least three independent forms of H_2 of strongly different equilibrium and kinetic properties.

2 Hydrogen states in samples quenched from high T

2.1 Quenched-in dimers At a high T (such as 1300 °C) the hydrogen impurity is in atomic form, most convincingly proved by the proportionality of the hydrogen solubility (on the order of 10^{16} cm^{-3}) to the square root of the H_2 pressure in the gas [14, 15]. Silicon is of intrinsic conductivity at high T, and it is generally accepted [4, 11] that the dominant charge state, in this case is H^+ in the bond-centered position (BC), with a small fraction of neutral hydrogen H^0 in the tetrahedral interstice (T). The electronic donor level of H in the BC state—for the H^0(BC)/H^+(BC) transition—is shallow [4] implying a negligible amount of H^0(BC), but the thermodynamic donor level for the H^0(T)/H^+(BC) transition may be located slightly above mid-gap [11] implying a small but appreciable amount of H^0(T) in intrinsic material. From now on, H^+ will refer to a BC state and H^0—to a T state.

One would expect that when boron-doped samples saturated with hydrogen at high T are quenched, the highly mobile H^+ species will be completely trapped by boron, to form neutral HB pairs (passivated boron). These defects can be monitored by IR spectroscopy [15–17] and by electrical measurements as well. It turned out however [17] that only a small fraction of the total hydrogen (~5%) is represented by HB at a moderate doping, with the boron concentration N_B around 10^{16} cm^{-3}. The HB fraction is higher at larger N_B [15, 18] and yet remains small. The major part of quenched-in hydrogen was found [17] to be in some dimeric form–denoted here H_{2A}—that gives rise to a weak IR band detectable in thick samples.

2.2 Conversion of quenched-in hydrogen dimers H_{2A} into HB By annealing at 160 °C, the quenched-in H_{2A} dimers gradually disappear with a simultaneous rise in the HB concentration [17]. The concentration sum of hydrogen in the two forms, [HB] + 2 [H_{2A}], remains constant and close to the SIMS-based total concentration. Conversion of H_{2A} into HB is complete at $N_B = 3 \times 10^{16}\,cm^{-3}$ but only partial at $N_B = 10^{16}\,cm^{-3}$. The initial loss (dissociation) rate of H_{2A} was found [17] to be proportional to the boron concentration, or equivalently to the hole concentration p. The dependence of the dissociation rate constant on the material parameters is defined by the type of the backward pairing reaction:

For $H^0 + H^0$ pairing path, the dissociation rate depends only on T.

For $H^0 + H^+$ pairing, the dissociation involves capturing a hole ($H_{2A} + h^+ \rightarrow H^0 + H^+$) and thus the dissociation rate is proportional to p. This hole-assisted dissociation does not require a two-stage process through a hypothetical intermediate $H_{2A}{}^+$ charge state. It rather implies that every time a hole encounters a neutral dimer, there is a probability of a dissociation into $H^0 + H^+$.

For the $H^+ + H^+$ reaction (retarded by Coulombic repulsion of these species), the dissociation involves capturing two holes, and the rate is proportional to p^2.

For more complicated pairing reactions like $H^0 + HB \rightarrow H_2 + B^- + h^+$ or $H^+ + HB \rightarrow H_2 + B^- + 2h^+$, the dissociation rate depends on both p and the non-passivated boron concentration $[B] = N_B - [HB]$. For the former pairing path, the H_2 dissociation rate is proportional to $[B]\,p$, while for the latter it is proportional to $[B]\,p^2$.

From this list it is clear that the observed H_{2A} dissociation is a reverse process to the pairing of H^+ and H^0–with a hole-assisted dissociation rate proportional to p. The variation in the H_{2A} concentration C_{2A} (and the related change in the HB concentration)—by dissociation and backward pairing—is then described by

$$dC_{2A}/dt = -\alpha_A(pC_{2A} - [H^+][H^0]/K_A), \quad (1)$$

where α_A is the dissociation rate coefficient and K_A is the equilibrium constant in the mass action law for dissociation/pairing. The two charge states of H are assumed to coexist in equilibrium:

$$[H^+]/[H^0] = p/p_d, \quad (2)$$

where p_d is the characteristic hole concentration—for the Fermi level coincident with the effective donor level for the H^0(T)/H^+(BC) transition.

The HB complex dissociates very quickly [19]—within 3 s at 160 °C—and hence H^+ and HB coexist in a strict equilibrium ratio corresponding to the mass action law for the trapping/releasing of H^+ by boron:

$$[H^+][B]/[HB] = K. \quad (3)$$

The equilibrium constant K for H^+ trapping/releasing is expressed as

$$K = (\rho/4)\exp(-E/kT), \quad (4)$$

where ρ is the lattice site density. The factor 4 stands for the 4 equivalent positions of H^+ around B. The binding energy E of H^+ to B^- is thought [3, 20] to be in a range of 0.6–0.8 eV, and we adopt the average value, 0.7 eV. An expected value of K at 160 °C is $\sim 10^{14}\,cm^{-3}$–much smaller than N_B. By Eq. (3), the $[H^+]/[HB]$ ratio is ~0.01. Hence the $H^+ + HB$ equilibrated sub-community of hydrogen is represented at this T, mostly by HB. The experimentally known variable is [HB] and it is convenient to re-write the rate Eq. (1) expressing [H^0] and [H^+] through [HB] from Eqs. (2) and (3):

$$dC_{2A}/dt = -\alpha_A(pC_{2A} - \chi_A([HB]/[B])^2/p). \quad (5)$$

The modified equilibrium constant χ_A is equal to $p_d K^2/K_A$. Equation (5) defines the evolution of C_{2A} and [HB] for specified total hydrogen concentration $C_{tot} = [HB] + 2\,C_{2A}$ and the total boron concentration $N_B = [HB] + [B]$. The hole concentration is $[B] - [H^+]$ and is close to [B]. When numerically solved, Eq. (5) well reproduces the observed time dependence of [HB] (Fig. 1) with the following best-fit parameters: $\alpha_A = 10^{-21}\,cm^3\,s^{-1}$ and $\chi_A = 4 \times 10^{46}\,cm^{-9}$.

After a prolonged annealing, the equilibrium between HB and H_{2A} is finally reached:

$$C_{2A} = \chi_A([HB]/[B])^2/p^2. \quad (6)$$

With a defined equilibrium constant χ_A, we can calculate by Eq. (6), the dependence of the final value of C_{2A} on N_B for any specified C_{tot}. The predicted—very strong—dependence (Fig. 2) is consistent with that reported [17]: about 50% of hydrogen remains in H_{2A} form at $N_B = 10^{16}\,cm^{-3}$ but almost nothing at $N_B = 3 \times 10^{16}\,cm^{-3}$.

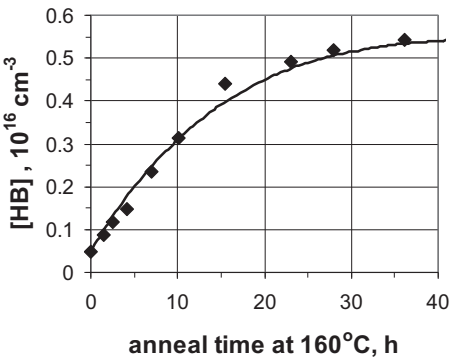

Figure 1 A rise in the HB concentration upon annealing quenched samples at 160 °C [17]. The boron concentration $N_B = 10^{16}\,cm^{-3}$, the total hydrogen $C_{tot} = 1.1 \times 10^{16}\,cm^{-3}$. The solid curve is a fit by Eq. (5) with $\alpha_A = 10^{-21}\,cm^3\,s^{-1}$ and $\chi_A = 4 \times 10^{46}\,cm^{-9}$.

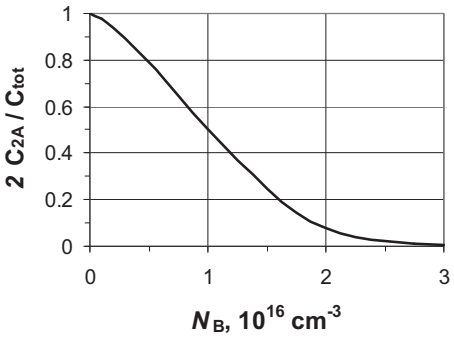

Figure 2 Final (equilibrium) fraction of hydrogen in the H_{2A} form at 160 °C in dependence of the boron concentration N_B, calculated by Eq. (6) with $C_{tot} = 1.1 \times 10^{16}\,cm^{-3}$.

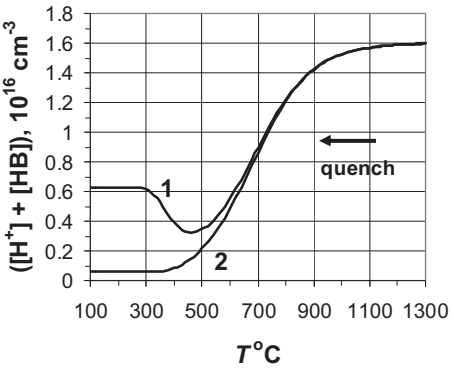

Figure 3 Evolution of the concentration $[HB] + [H^+]$ of single-hydrogen species in the course of quenching from 1300 °C, with $C_{tot} = 1.6 \times 10^{16}\,cm^{-3}$, calculated by Eq. (5); the assumed quench rate is $500°s^{-1}$. The curves 1 and 2 are for $N_B = 10^{17}$ and $10^{16}\,cm^{-3}$, respectively.

A conversion of quenched-in H_{2A} into HB was observed also at 175 °C [15] in a sample with $N_B = 10^{17}\,cm^{-3}$; now the dissociation of H_{2A} proceeds much faster due to both a higher p and a higher α_A in Eq. (5). The deduced value is $\alpha_A = 3.2 \times 10^{-21}\,cm^3\,s^{-1}$. The two known values of this parameter for 160 and 175 °C, yield the following Arrhenius type temperature dependence:

$$\alpha_A = (1.3 \times 10^{-6} cm^3\,s^{-1}) \exp(-1.3\ eV/kT). \qquad (7)$$

2.3 Redistribution between H_{2A} and HB during a quench The time evolution of HB and H_{2A} in the course of a quench from the saturation temperature (1300 °C) can be simulated by solving Eq. (5) with temperature-dependent parameters α_A, χ_A, and K. For that we need the activation energy E_A of the equilibrium constant χ_A, and calculations were made for different values of E_A. The computed quenched-in value of [HB] is only slightly sensitive to the cooling rate—tentatively taken to be $500°s^{-1}$ [21]—but strongly sensitive to E_A. In Fig. 3, curve 1, an example of the simulated evolution of single-hydrogen concentration $C = [H^+] + [HB]$ is shown for $C_{tot} = 1.6 \times 10^{16}\,cm^{-3}$ and $N_B = 10^{17}\,cm^{-3}$—the values from Refs. [18, 21]. Initially (at high T) the concentration C_{2A} is small, but the H_{2A} species becomes dominant in the intermediate temperature range of a quench, around 400 °C—which is manifested by a strong reduction in $[H^+] + [HB]$ (Fig. 3). At still lower T, when HB dominates over H^+, there is a pronounced redistribution from H_{2A} to HB that occurs even at a very fast cooling. This is caused by a gain in the energy due to the binding of dissociation-produced H^+ by boron. The finally achieved (as-quenched) [HB] is about $6 \times 10^{15}\,cm^{-3}$ [18, 21], and this number is reproduced with $E_A = 1.7$ eV (curve 1 in Fig. 3). Now the Arrhenius-type dependence of the equilibrium dissociation constant χ_A is defined:

$$\chi_A = (2.35 \times 10^{66} cm^{-9}) \exp(-1.7\ eV/kT). \qquad (8)$$

With specified $\chi_A(T)$, one can calculate the evolution of $[H^+] + [HB]$ during a quench for any N_B and C_{tot}. The curve 2 in Fig. 3 is for a lower boron concentration, $N_B = 10^{16}\,cm^{-3}$; here a quenched-in [HB] is very small in agreement with the reported data [17].

2.4 Out-diffusion of quenched-in dimers A loss kinetics of hydrogen in hydrogen-saturated quenched samples has been monitored [22] using a radioactive hydrogen isotope (tritium). The temperature range of annealing was 400–500 °C. The tritium loss is by out-diffusion and subsequent evaporation into the ambient. The loss proceeds in two distinct stages, a fast one and a slow one, which corresponds to out-diffusion of two independent tritium species. The total amount M_1 of the first species of a diffusivity D_1 is obtained by solving the diffusion equation [22]:

$$M_1/M_{10} = (8/\pi^2)\Sigma(1/k^2)\exp(-(k\pi/d)^2 D_1 t), \qquad (9)$$

where the sum is over odd k, d is the sample thickness, and M_{10} is the initial amount. A similar equation holds for the second component. The reported time dependence of the total remaining fraction $M/M_0 = (M_1 + M_2)/(M_{10} + M_{20})$ is well reproduced for each T by setting proper values for D_1, D_2, and the initial fraction $f_2 = M_{20}/M_0$ of the second (slow) component. The values of D_2 and f_2 are determined by a long tail in the tritium loss curve, and then there is a unique value of D_2 (within about 10%) to fit the fast portion of the loss curve. The two deduced diffusivities, $D_1 = D_f$ (for the fast stage) and $D_2 = D_s$ (for the slow stage) have been then converted into the diffusivity of hydrogen by multiplying by a square root of the mass ratio of the two isotopes, $3^{1/2}$. Both D_f and D_s—shown in Fig. 4—are remarkably smaller than the atomic hydrogen diffusivity measured by Van Wieringen and Warmolz [14] and extrapolated to the present T range (about $2.5 \times 10^{-6}\,cm^2 s^{-1}$ at 400 °C).

The interpretation of these results is straightforward, with the now specified properties of H_{2A} dimers. The dissociation time of H_{2A} is $1/(\alpha_A\,p)$. The inspected samples were lightly

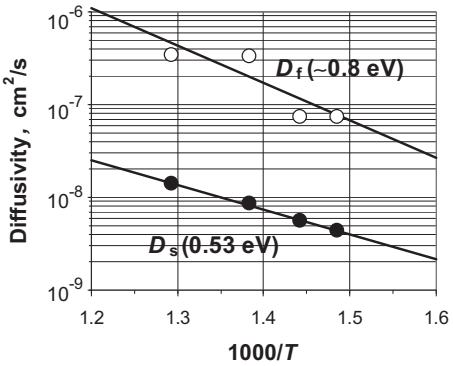

Figure 4 Apparent hydrogen diffusivity for the fast and slow components of tritium loss from quenched samples, deduced from the loss curves reported in Ref. [22].

doped, and the hole concentration p is of the intrinsic value, $2 \times 10^{16}\,\mathrm{cm}^{-3}$ at 400 °C. The H_{2A} dissociation time is then 0.1 s. This means that there is a strict equilibrium between H_{2A} and H^+ described by Eq. (6) that can be re-written in a more useful form through $C^+ = [H^+]$ instead of [HB] since H^+ dominates over HB at $T \geq 400$ °C:

$$(C^+)^2/C_{2A} = K_{\mathrm{eff}} = (pK)^2/\chi_A. \qquad (10)$$

The effective dissociation constant K_{eff} is $6 \times 10^{12}\,\mathrm{cm}^{-3}$ at 400 °C—far smaller than the total hydrogen concentration C_{tot} (which was not specified in [22] but should be in a range 10^{15} to $10^{16}\,\mathrm{cm}^{-3}$). Hence, the equilibrated community of H_{2A} and H^+ is represented mostly by the dimers H_{2A}, with only a small fraction of atomic hydrogen. An apparent hydrogen diffusivity will be then much smaller than that of atomic hydrogen.

On the other hand, D_f is much larger (by a factor of about 100) than the diffusivity of H_{2A} discussed in the next subsection. It means that the out-diffusion of the equilibrated $H_{2A} + H^+$ community is controlled mostly by a minor but fast atomic component. The diffusion flux is $J = -(D^+ + D^0 p_d/p)\mathrm{d}C^+/\mathrm{d}z$, taking into account a transport by both H^+ and H^0. The minor component H^0 can be yet of a higher diffusivity D^0 in comparison to D^+. If $\mathrm{d}C^+/\mathrm{d}z$ is expressed through the gradient of $C_{\mathrm{tot}} = 2\,C_{2A}$, the flux is equal to $-D_{\mathrm{eff}}\ \mathrm{d}C_{\mathrm{tot}}/\mathrm{d}z$, where the effective (apparent) diffusivity of the $H_{2A} + H^+ + H^0$ community is

$$D_{\mathrm{eff}} = (D^+ + D^0 p_d/p)\left(K_{\mathrm{eff}}/(8\ C_{\mathrm{tot}})\right)^{1/2}. \qquad (11)$$

The diffusivity of monoatomic hydrogen $D^+ + D^0\ p_d/p$ is found by extrapolation of the Van Wieringen and Warmolz data [14], and it is far larger than the diffusivity of H^+ [3] based on the data of Ref. [23]. It implies that the major contribution into the atomic diffusivity in intrinsic Si is by H^0. The resulting estimate for D_{eff} (400 °C) by Eq. (11) is $\sim 5 \times 10^{-8}\,\mathrm{cm}^2\,\mathrm{s}^{-1}$, close to the absolute value of D_f in Fig. 4. The activation energy for D_{eff} resulting from Eq. (11) is about 0.9 eV. The points for D_f in Fig. 4 are strongly scattered, but not inconsistent with this value.

We can now safely conclude that the fast component of hydrogen (tritium) loss corresponds to a transport of H_{2A} mediated by the atomic species H^+ and H^0 (mostly H^0) which are present in equilibrium with H_{2A}. The slow component is then out-diffusion of some other hydrogen species, definitely not monomeric. Accordingly, the most natural attribution of the slow component is to another kind of dimer (denoted H_{2B}) which does not dissociate at all on the time scale of the loss curve. The diffusivity D_{2B} of H_{2B} is identical to D_s:

$$D_{2B} = D_s = (0.00004\ \mathrm{cm}^2\,\mathrm{s}^{-1})\exp(-0.53\mathrm{eV}/kT). \qquad (12)$$

The implication of the above consideration is that a sample—saturated with hydrogen at high T and quenched—actually contains not one kind of hydrogen dimer (H_{2A}) but two H_{2A} and H_{2B}. The H_{2A} species are manifested by an IR band but the H_{2B} species remain "hidden." This may account for a difference in the concentration of HB achieved after complete conversion of H_{2A} into HB for two annealing temperatures, 160 and 175 °C. At 160 °C and $N_B = 3 \times 10^{16}\,\mathrm{cm}^{-3}$, the achieved [HB] is $1.1 \times 10^{16}\,\mathrm{cm}^{-3}$ [17] while at 175 °C and $N_B = 10^{17}\,\mathrm{cm}^{-3}$ it is remarkably higher, $1.6 \times 10^{16}\,\mathrm{cm}^{-3}$ [15, 21]. We can attribute this difference to the initial presence of non-detectable H_{2B} dimers which do not dissociate at 160 °C (thus remaining hidden) but do dissociate at a higher temperature of 175 °C (and at a higher N_B) thus contributing into [HB]. The conclusion is that as-quenched samples of moderate N_B contain about $10^{16}\,\mathrm{cm}^{-3}$ of hydrogen in the H_{2A} form and $5 \times 10^{15}\,\mathrm{cm}^{-3}$ in the H_{2B} form.

2.5 Trapping of quenched-in dimers at low T

Annealing of hydrogen-saturated quenched samples slightly above T_{room} leads to the appearance of a new IR band [24] convincingly shown to result from the trapping of quenched–in hydrogen dimers by oxygen. From these data, the product of the dimeric diffusivity and the capture radius r was deduced [24], and with a reasonable assumption about the value of $r \approx 0.3$ nm, the dimeric diffusivity is about $5 \times 10^{-17}\,\mathrm{cm}^2\mathrm{s}^{-1}$ at 30 °C; the activation (migration) energy is about 0.78 eV. Both the absolute value and the migration energy are essentially different from those of H_{2B} as given by Eq. (12), and therefore the dimers traced in ref. [24] should be identified as H_{2A}. Hence,

$$D_{2A} \approx (4.6 \times 10^{-4}\mathrm{cm}^2\,\mathrm{s}^{-1})\exp(-0.78\mathrm{eV}/kT). \qquad (13)$$

The kinetic and equilibrium properties of H_{2A} dimers—the dissociation coefficient α_A, the equilibrium constant χ_A and the diffusivity D_{2A}—are now completely specified by Eqs. (7), (8), and (13). For the other kind of hydrogen dimer, H_{2B} only the diffusivity was specified. It is not even clear by what pairing reaction the H_{2B} are produced. Since, these species do not dissociate at 400 °C at a low N_B but

presumably dissociate at 175 °C at higher N_B and p, it is likely that the pairing path involves HB species and could be $H^+ + HB \rightarrow H_{2B} + B^- + 2h^+$, which implies that the dissociation rate is proportional to [B] p^2, and for this reason can be higher at lower T but at much higher N_B and p.

3 Dimers in plasma-exposed samples

3.1 Relaxed hydrogen profiles in lightly doped n-Si Hydrogen depth profiles in p-Si samples exposed to plasma, normally in a range of 120–200 °C, are often of a complicated shape [1–3, 25–27], including a flat portion where boron is completely passivated and the hydrogen concentration is identical to N_B. The situation is much simpler in lightly doped n-Si where donor passivation is not pronounced. Upon switching off the plasma source of hydrogen, the induced hydrogen profile relaxes by simple out-diffusion [27]. The deduced diffusivity is very close to D_{2A} as defined by Eq. (13), both by the activation energy (0.8 eV) and by the absolute value. It is thus clear that hydrogen is incorporated from plasma into lightly doped n-Si as predominantly H_{2A} dimeric species. The diffusivity deduced by profile relaxation [27] refers to deuterium. If recalculated to the case of hydrogen (multiplying it by the square root of the isotope mass ratio, here $2^{1/2}$) it is equal to

$$D_{2A} = (0.001\ \mathrm{cm^2\,s^{-1}})\exp(-0.8\ \mathrm{eV}/kT). \quad (14)$$

The two expressions (13) and (14) refer to two different well separated T-ranges but they are almost identical.

Since the dissociation of H_{2A} is by $H_{2A} + h^+ \rightarrow H^0 + H^+$ reaction, it is completely suppressed in n-Si due to a lack of holes. This accounts for a simple out-diffusion of H_{2A} dimers—not involving a transport by the atomic component of hydrogen, contrary to the case of $T \geq 400$ °C.

3.2 In-diffused slow dimers In-diffused hydrogen profiles almost always contain a narrow near-surface region of a high concentration [25–27]. This part of the profile is normally attributed to the hydrogen accumulation in a thin plasma-damaged region. However, there is a clear evidence against this notion. The in-diffusion profiles produced at 200 °C for various exposure times [28] show (Fig. 5) a standard wide plateau where the hydrogen concentration is equal to $N_B = 10^{18}$ $\mathrm{cm^{-3}}$—a region where boron is completely converted into HB. In addition, there is a near-surface high-concentration part that spreads with time in proportion to $t^{1/2}$ and the shape of this part is well described by an erfc function (the solid lines in Fig. 5). This clearly shows that the near-surface part is due to in-diffusion of some very slow species; the diffusivity obtained by fitting the three profiles in Fig. 5 is close to $2.5 \times 10^{-14}\,\mathrm{cm^2\,s^{-1}}$. For comparison, $D_{2A} = 2 \times 10^{-12}\,\mathrm{cm^2\,s^{-1}}$ at this T and D_{2B} is still larger.

This result is interpreted as existence of one more dimeric species (H_{2C}), which is a very slow diffuser.

Near-surface high-concentration parts—similar to those shown in Fig. 5—are observed also at lower T [25-27], but they are not so well resolved. The temperature dependence of D_{2C} is better specified by assuming a reasonable prefactor of $0.001\,\mathrm{cm^2\,s^{-1}}$. Then, a tentative expression for the temperature-dependent D_{2C} (for ^1H isotope) is

$$D_{2C} \approx (0.0016\ \mathrm{cm^2\,s^{-1}})\exp(-1\ \mathrm{eV}/kT). \quad (15)$$

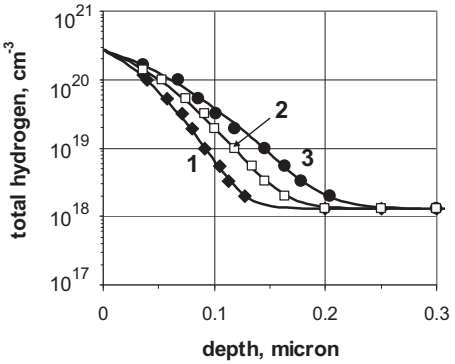

Figure 5 Hydrogen (deuterium) depth profiles [28] in samples with $N_B = 10^{18}\,\mathrm{cm^{-3}}$ exposed to plasma at 200 °C for 5, 10, and 15 min (curves 1–3, respectively). The solid curves are fitted erfc-like profiles, and the deduced diffusivity is $2.5 \times 10^{-14}\,\mathrm{cm^2\,s^{-1}}$.

3.3 Slow dimers produced in an n–p structure A strong support of existence of slow H_{2C} dimers comes from a hydrogen profile [25, 26] in an n–p structure created by implantation of phosphorus into boron-doped sample. The structure includes a near-surface n-region, a bulk p-region and an intermediate space charge region that can be strongly expanded by an applied bias. After 200 °C/1 h exposure, the hydrogen profile (Fig. 6) shows a concentration well exceeding $N_B = 10^{17}\,\mathrm{cm^{-3}}$ within the p-region—indicating local formation of hydrogen dimers. These dimers do not penetrate much to the left into the adjacent space charge region, and the estimated diffusivity is less than $3 \times 10^{-14}\,\mathrm{cm^2\,s^{-1}}$. A reasonable conclusion is that hydrogen dimers produced within the p-region are the slow species H_{2C}.

The formation process is as follows. The neutral hydrogen H^0 penetrates into the p-region from the sample surface—through the n-region and the space charge region. In the hole-populated p-region it converts into H^+, and this species is involved in the production of H_{2C}. Different pairing paths (listed in Section 2.1) have been tried; it turned out that the best reproduction of the profile shape is for the pairing reaction $H^+ + HB \rightarrow H_{2C} + B^- + 2h^+$. Along with H_{2C}, also H_{2A} species may be produced according to Eq. (5) but these mobile dimers quickly out-diffuse and give only a small contribution into the total hydrogen concentration within the p-region.

The total concentration of the single-hydrogen species, $C = [HB] + C^+$, changes by two processes.

The first one is the diffusion of H^+ and H^{00} (their concentrations C^+ and C^{00} are related by Eq. [2]):

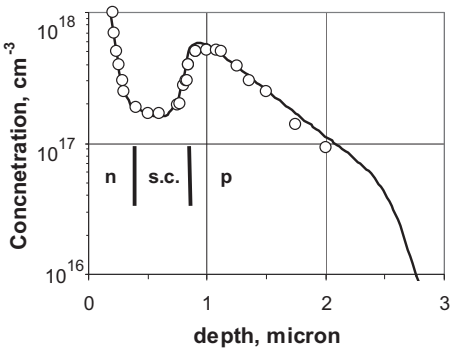

Figure 6 Hydrogen (deuterium) depth profile [25, 26] in an n-p structure with $N_B = 10^{17}\,cm^{-3}$ exposed to plasma at 200 °C for 1 h, under a bias of 10 V. The solid curve is a simulated profile (see the text).

$$\partial C/\partial t = -\partial J/\partial z,$$
$$J = -(D^0 + D^+ p/p_d)\partial C^0/\partial z. \quad (16)$$

The flux J of monoatomic species includes a drift of H^+ in the electric field related to a space variation in p. For calculation, it is convenient to use a variable $Y = C^{00}/p_d = C^+/p$. The concentration C^+, for a specified C is defined by the equation $C = N_B\,C^+/(C^+ + K) + C^+$ and the hole concentration is $p = [B] - [H^+] = N_B\,K/(C^+ + K) - C^+$. The boundary condition is a fixed incoming flux J at the left edge of the p-region; this is a fitting parameter.

The second process is a loss of C due to formation of H_{2C} dimers:

$$\partial C_{2C}/\partial t = -\beta_C\left((C^+/K)[HB] - C_{2C}[B]p^2/\chi_C\right), \quad (17)$$

where β_C is the kinetic coefficient for the $H^+ + HB$ reaction and χ_C is the equilibrium constant similar to χ_A in Eq. (5). The derivative $\partial C/\partial t$, due to the production of H_{2C} by reaction (17), is $-2\partial C_{2C}/\partial t$. The ratio C^+/K is equal to [HB]/[B]. Boron was found [26] to be strongly passivated within the p-region which corresponds to a large local value of C^+/K. In simulations, we will neglect backward dissociation of produced H_{2C} which is true if χ_C is sufficiently large – meaning a high stability of H_{2C}.

Beside these two equations, there is also a diffusion equation for H_{2C}:

$$\partial C_{2C}/\partial t = D_{2C}\partial^2 C_{2C}/\partial z^2. \quad (18)$$

For the diffusivity D_{2C}, we adopt a value $2.5 \times 10^{-14}\,cm^2\,s^{-1}$ deduced from the deuterium profiles of Fig. 5.

The total time derivative of each variable, C and C_{2C}, is composed of all the contributions resulting from Eqs. (16)–(18). The computed profile of the total hydrogen concentration, $C_{tot} = C + 2\,C_{2C}$, is sensitive mostly to the assumed incoming flux J, the kinetic coefficient of pairing β_C, and the product D^+K. A variation in other parameters ($D^{00}p_d$ and D^+), even if strong can be adjusted by a slight change in the three basic parameters. The best-fit computed profile shown by the solid line in Fig. 6 corresponds to $J = 10^{10}\,cm^{-2}\,s^{-1}$, $\beta_C = 6 \times 10^{-5}\,s^{-1}$, and $D^+K = 2 \times 10^4\,cm^{-1}\,s^{-1}$. The diffusivity D^+ was taken to be $10^{-8}\,cm^2\,s^{-1}$ [3, 23] based on the data for the jump rate of H^+ between the neighboring BC sites at low T. The product D^0p_d was tentatively taken to be $10^6\,cm^{-1}s^{-1}$. The value of C_{tot} within the space charge region (marked s.c. in Fig. 6—to the left of the p-region) is attributed to in-diffusion of H_{2A} from the sample surface —which is a common effect in n-Si. The near-surface concentration C_{2A} was adjusted to be $1.25 \times 10^{17}\,cm^{-3}$. Finally, a narrow high-concentration region in Fig. 6 was treated as in-diffusion of H_{2C} from the surface (similar to that shown in Fig. 5); the near-surface concentration C_{2C} was adjusted to be $6 \times 10^{18}\,cm^{-3}$.

4 Formation of H_{2C} dimers by annealing quenched samples

4.1 Isothermal annealing Annealing of quenched samples at 175 °C [15] results, as discussed above in a fast conversion of H_{2A} (and probably also of H_{2B}) into HB and accordingly in a fast rise in [HB], up to the total hydrogen concentration inherited from a high T (1300 °C). A more prolonged anneal leads to a gradual reduction in [HB] to a new saturated value (Fig. 7). This effect can be naturally attributed to a slow formation of stable H_{2C} dimers which finally come into equilibrium with HB. The solid line in Fig. 7 was obtained by solving Eqs. (5) and (16), with the following best-fit parameters of H_{2C}: $\beta_C = 7.5 \times 10^{-6}\,s^{-1}$, $\chi_C = 5.25 \times 10^{51}\,cm^{-6}$. By two known values of β_C— at 200 and 175 °C—one can specify the Arrhenius-type temperature dependence of this pairing coefficient

$$\beta_C = (5.5 \times 10^{11}\,s^{-1})\exp(-1.5/kT). \quad (19)$$

4.2 Isochronal annealing Isochronal annealing [18] in a range 100–375 °C for 30 min (with a step of 25 centigrade) leads initially to a rise in [HB] to the total hydrogen concentration, with a peak at around 200 °C (Fig. 8). At higher T, there is a drop in [HB] that can be attributed to redistribution from HB to H_{2A} and also to formation of stable H_{2C} dimers. The redistribution alone—described by Eq. (5) with known temperature-dependent parameters α_A and χ_A—results in a computed curve 1 in Fig. 8 which is well above the experimental points. This shows an importance of H_{2C} formation, to account for a strong reduction in [HB] at $T > 200$ °C. When both reactions—the redistribution process by Eq. (5) and H_{2C} formation by Eq. (17) with neglected backward dissociation—are taken into account, the computed [HB] evolution (curve 2 in Fig. 8) is close to the experimental points. However, to get this close fit, the temperature dependence of the kinetic coefficient β_C should be modified—assuming the activation energy 1.1 eV instead of 1.5 eV in Eq. (19).

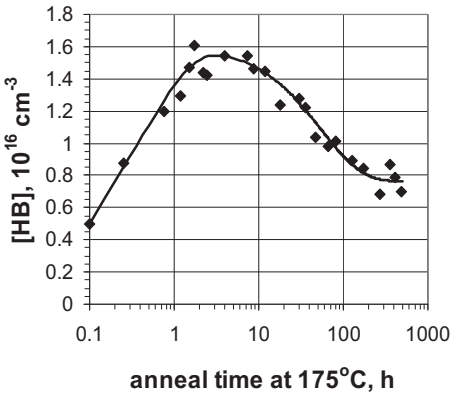

Figure 7 Evolution of the HB concentration upon annealing quenched samples at 175 °C [15]. The boron concentration $N_B = 10^{17}\,cm^{-3}$, the total hydrogen $C_{tot} = 1.6 \times 10^{16}\,cm^{-3}$. The rising part of the solid curve is a fit by Eq. (5), and the dropping part—by Eq. (17) with $\beta_C = 7.5 \times 10^{-6}\,s^{-1}$ and $\chi_C = 5.25 \times 10^{51}\,cm^{-9}$.

5 Hydrogen concentration introduced by firing of solar cells Solar cell fabrication includes a firing step in a belt furnace, with a peak temperature at around 750 °C. This treatment is believed to incorporate hydrogen [5, 6]. The presence of hydrogen is most convincingly proved by the effect of isochronal annealing on the subsequently measured rate constant R_{de} of the permanent deactivation of the boron–oxygen centers [6]: the evolution of R_{de} is very similar to that of [HB] in Fig. 8. This shows that R_{de} is controlled by the concentration of HB defects (through the released monoatomic hydrogen in equilibrium with HB). The ratio of the initial and peak values of R_{de} (about 0.44 [6]) is then equal to the ratio of as-quenched and peak values of [HB]; the latter is the total hydrogen content. Therefore, the ratio of the two [HB] values is identical to the fraction of quenched-in [HB] in the HB + H_{2A} community.

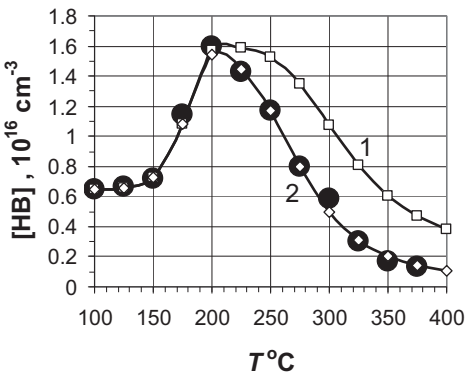

Figure 8 Variation in the concentration of HB by isochronal anneal for 30 min with a step of 25 °C [18] (large circles); the boron concentration $N_B = 10^{17}\,cm^{-3}$, the total hydrogen $C_{tot} = 1.6 \times 10^{16}\,cm^{-3}$. The simulated curve 1 is for the HB + H_{2A} subsystem, and the curve 2—for HB + H_{2A} + H_{2C} system.

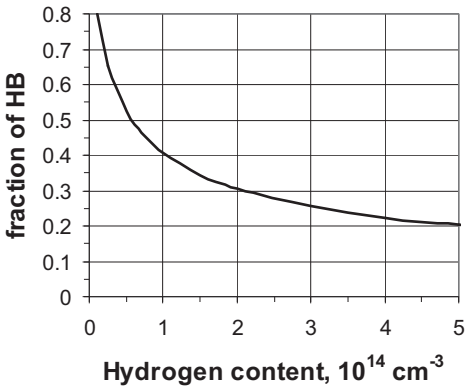

Figure 9 Calculated fraction of the HB state in fired samples (the peak temperature is 750 °C, the cooling-down rate is $100°s^{-1}$) for a sample with $N_B = 10^{16}\,cm^{-3}$, in dependence of the total hydrogen content in the single-hydrogen (H^+ + HB) and H_{2A} states.

This fraction, computed by solving Eq. (5), is shown in Fig. 9 in dependence of the total hydrogen concentration C_{tot}, for a representative boron concentration of $10^{16}\,cm^{-3}$ and a representative cooling rate of $100°s^{-1}$ [29]. The quenched-in fraction of 0.44 corresponds to $C_{tot} = 8 \times 10^{13}\,cm^{-3}$, and this number gives a reasonable estimate of the hydrogen concentration in fired samples (and in solar cells).

6 Summary Various experimental data have been analyzed in this work in a particular sequence to provide a continuous logical chain showing existence of three different and independent diatomic species of hydrogen:

H_{2A}—metastable dimers of a moderate diffusivity created by quenching from a high T, and also by in-diffusion from the surface during exposure to a plasma at low T. The pairing reaction to create H_{2A} in p-Si is $H^+ + H^{00} \rightarrow H_{2A} + h^+$.

H_{2B}—metastable dimers of a high diffusivity created by quenching—but with no sign of their presence in plasma-treated samples. The pairing reaction cannot be specified yet, but most likely it involves a reaction of atomic hydrogen with HB complex (passivated boron).

H_{2C}—stable dimers of a low diffusivity that, during exposure to a plasma, in-diffuse from the surface, and also can be generated in the sample bulk. These species are also produced by annealing samples quenched from high T. The pairing reaction to create H_{2C} is most likely $H^+ + HB \rightarrow H_{2C} + B^- + 2h^+$.

The deduced kinetic properties of these three dimers cannot shed a light on their arrangement on the atomic scale. It is believed [17] that H_{2A} is a hydrogen molecule within a tetrahedral interstice. By electron irradiation, this species is converted [21, 30] into a so-called H_2^* defect [11] in which two hydrogen atoms are located at two opposite sides of a silicon atom, along ⟨111⟩ direction. This defect gives distinct IR bands, and for this reason it cannot be identified with H_{2B}—since the H_{2B} (present in quenched samples) is optically inactive. It is reasonable to identify H_2^* as H_{2C},

otherwise we would have four (probably too many) different dimeric species.

The active hydrogen species important for the material properties is atomic hydrogen co-existing in equilibrium with trapped hydrogen HB in boron–doped material. It is then the HB concentration that controls the hydrogen effects, and in particular the permanent deactivation of boron–oxygen centers that degrade the lifetime and hence the solar cell efficiency. By the simulated dependence of quenched-in [HB] on the total hydrogen concentration, we were able to estimate the total hydrogen concentration in fired solar cells to be $\sim 10^{14} \mathrm{cm}^{-3}$.

References

[1] J. I. Pankove, R. O. Wance, and J. E. Berkeyheiser, Appl. Phys. Lett. **45**, 1100 (1984).
[2] S. J. Pearton, Mater. Sci. Eng. B **23**, 130 (1994).
[3] C. Herring, N. M. Johnson and, Van de walle, Phys. Rev. B **64**, 125209–125201 (2001).
[4] S. K. Estreiher, M. Stavola, and J. Weber, in: Silicon, Germanium, and their Alloys: Defects, Impurities and Nanocrystals, edited by G. Kissinger and S. Pizzini (CRC Press, Boca Raton, 2014), chap. 7.
[5] S. Wilking, A. Herguth, and G. Hahn, Energy Proc. **38**, 642 (2013).
[6] S. Wilking, C. Beckh, S. Ebert, A. Herguth, and G. Hahn, Sol. Energy Mater. Sol. Cells **131**, 228 (2014).
[7] V. V. Voronkov and R. Falster, Phys. Status Solidi B **253**(9), 1721 (2016).
[8] H. Fischer and W. Pshunder, in: Proc. 10-th IEEE Photovolataic Conference, 404 (1973).
[9] K. Bothe and J. Schmidt, J. Appl. Phys. **99**, 013701 (2006).
[10] V. V. Voronkov and R. Falster, J. Appl. Phys. **107**, 053509 (2010).
[11] K. J. Chang and D. J. Chadi, Phys. Rev. B **40**, 11644 (1989).
[12] J. D. Holbech, B. Bech, Nielsen, R. Jones, P. Sitch, and S. Oberg, Phys. Rev. Lett. **71**(6), 875 (1993).
[13] A. R. Peaker, V. P. Markevich, and L. Dobaczewski, in: Defects in Microelectronic Materials and Devices, edited by D. M. Fleetwood, S. T. Pantelides, and R. D. Schrimpf (CRC Press, Boca Raton, 2009), p. 27.
[14] A. Van Wieringen and N. Warmoltz, Physica **22**, 849 (1956).
[15] M. J. Binns, R. C. Newman, S. A. MaQuaid, and E. C. Lightowlers, Mater. Sci. Forum. **861**, 143–147 (1994).
[16] N. M. Johnson, Phys. Rev. B **31**(8), 5525 (1985).
[17] R. E. Pritchard, J. H. Tucker, R. C. Newman, and E. C. Lightowlers, Semicond. Sci. Technol. **14**, 77 (1999).
[18] S. A. McQuaid, M. J. Binns, and R. C. Newman, Appl. Phys. Lett. **62**(14), 1612 (1993).
[19] T. Zundel and J. Weber, Phys. Rev. B **39**(18), 13549 (1989).
[20] C. P. Herrero, M. Stutzmann, A. Breitschwerdt, and P. V. Santos, Phys. Rev. B **41**(2), 1054 (1990).
[21] M. J. Binns, S. A. McQuaid, R. C. Newman, and E. C. Lightowlers, Semicond. Sci. Technol. **8**, 1908 (1993).
[22] T. Ichimiya and A. Furuichi, Int. J. Appl. Radiat. Isotopes **19**, 573 (1968).
[23] Gorelkinskii Yu V and N. N. Nevinnyi, Mater. Sci. Eng. B **36**, 133 (1996).
[24] V. P. Markevich and M. Suezawa, J. Appl. Phys. **83**(6), 2988 (1998).
[25] N. M. Johnson and C. Herring, Phys. Rev. B **38**, 1581 (1988).
[26] C. Herring and N. M. Johnson, Semicond. Semimetals **34**, 225 (1991).
[27] N. M. Johnson and C. Herring, Phys. Rev. B **43**(17), 14297 (1991).
[28] B. Y. Tong, X. W. Wu, G. R. Yang, and S. K. Wong, Can. J. Phys. **67**, 379 (1989).
[29] D. C. Walter, B. Lim, K. Bothe, R. Falster, V. V. Voronkov, and J. Schmidt, Sol. Energy Mater. Sol. Cells **131**, 51 (2014).
[30] I. A. Veloarisoa, M. Stavola, D. M. Kozuch, R. E. Reale, and G. D. Watkins, Appl. Phys. Lett. **59**(17), 2121 (1991).

